

# INCIDENTAL POLYSEMANTICITY: A NEW OBSTACLE FOR MECHANISTIC INTERPRETABILITY

**Anonymous authors**

Paper under double-blind review

## ABSTRACT

Polysemantic neurons – neurons that activate for a set of unrelated features – have been seen as a significant obstacle towards interpretability of task-optimized deep networks, with implications for AI safety. The classic origin story of polysemanticity is that the data contains more “features” than neurons, such that learning to perform a task forces the network to co-allocate multiple unrelated features to the same neuron, endangering our ability to understand networks’ internal processing. In this work, we present a second and non-mutually exclusive origin story of polysemanticity. Specifically, we show that polysemanticity can arise incidentally, even when there are ample neurons to represent all features in the data, a phenomenon we term *incidental polysemanticity*. Using a combination of theory and experiments, we show that incidental polysemanticity can arise due to multiple reasons including regularization and neural noise; this incidental polysemanticity occurs because random initialization can, by chance alone, initially assign multiple features to the same neuron, and the training dynamics then strengthen such overlap. Our paper concludes by calling for further research quantifying the performance-polysemanticity tradeoff in task-optimized deep neural networks to better understand to what extent polysemanticity is avoidable.

## 1 INTRODUCTION

Deep neural networks are widely regarded as difficult to mechanistically understand, especially at the massive scales of modern frontier models. Such lack of interpretability is increasingly viewed as a serious concern in AI Safety since highly capable models might behave in unpredictable and undesirable ways (Hendrycks et al., 2023; Ngo et al., 2022). One outstanding challenge preventing better mechanistic interpretability of networks is *polysemanticity*, a phenomenon whereby individual neurons activate for unrelated input “features” (Olah et al., 2017; 2020). This phenomenon, why it occurs and how to interpret networks’ computation nonetheless has also been studied for decades by neuroscientists under the term of “mixed selectivity”, e.g., (Asaad et al., 1998; Mansouri et al., 2006; Warden & Miller, 2007; Rigotti et al., 2013; Barak et al., 2013; Raposo et al., 2014; Fusi et al., 2016; Parthasarathy et al., 2017; Lindsay et al., 2017; Zhang et al., 2017; Johnston et al., 2020).

A leading hypothesis for why neural networks learn polysemantic representations is out of necessity: if a task contains many more features than the number of neurons, then achieving high performance at the task might force the network to co-allocate unrelated features to the same neuron (Elhage et al., 2022). While intuitive and persuasive, in this work, we propose a second and non-mutually exclusive hypothesis: that polysemanticity might be caused by non-task factors in the training process. As such factors are not necessary to perform the task well, we call this form *incidental polysemanticity*.

In this paper, we study two non-task factors that could produce incidentally polysemantic representations:  $l_1$  regularization and neural noise. We hypothesize that the mechanism of neural network convergence from randomly initialized weight is contingent on the very slight correlation of certain neurons with useful features<sup>1</sup>. Gradient descent in the initial steps will amplify this correlation until the feature is accurately represented in the model weights. Suppose activations are incentivized to be sparse, as in the regularization setting. In this case, features will be represented by

<sup>1</sup>Formally, the neuron’s activation is correlated with whether the feature is present in the input (where the correlation is taken over the data points).

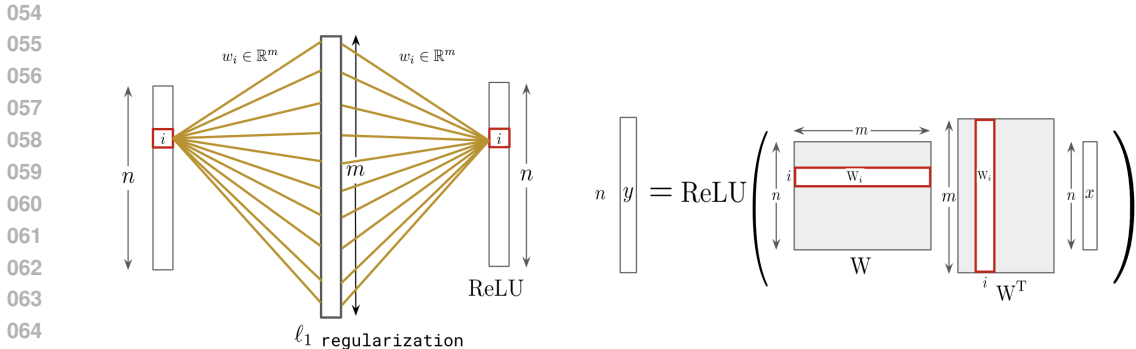


Figure 1: A visualization of the non-linear autoencoder setup with tied weights  $W \in \mathbb{R}^{n \times m}$ , a single hidden layer of size  $m$ ,  $l_1$  regularization with parameter  $\lambda$ , and a ReLU on the output layer.

a winner-take-all single neuron as opposed to a linear combination of neurons Oster et al. (2009).<sup>2</sup> When a winner-take-all dynamic is present, the neuron that is initially most correlated with the given feature will be the neuron that wins out and represents the feature when training completes. We term single neuron multi-feature representation arising from the aforementioned mechanism as *incidental polysemanticity*.

To illustrate the frequency at which incidental polysemanticity may arise, suppose that we have  $n$  useful features to represent and  $m \geq n$  neurons to represent them with (so that it is theoretically possible for each feature to be represented by a different neuron). By symmetry, the probability that the  $i^{\text{th}}$  and  $j^{\text{th}}$  feature are correlated with the same neuron, a *collision*, is exactly  $1/m$ . As there are  $\binom{n}{2} = n(n-1)/2$  pairs of features, we should expect  $\binom{n}{2} \times \frac{1}{m} = \frac{n(n-1)}{2m} = \Theta\left(\frac{n^2}{m}\right)$  collisions<sup>3</sup>.

Our experiments in small autoencoders demonstrate empirically this phenomenon, by which a constant fraction of collisions results in polysemantic neurons, despite the abundance of neurons not necessitating polysemanticity. Our main contributions are as follows:

- We describe two simple models which exhibit incidental polysemanticity: one based on  $l_1$  regularization (Section 2) and the other based on neural noise (Section 3).
- We study their sparsity and winner-take-all dynamics in mathematical detail, explore what happens over training when features collide, and confirm experimentally that the number of polysemantic neurons that are produced is a precise asymptotic match.
- In Section 4, we demonstrate that despite strong differences in their mathematical foundation and polysemantic configurations, the models share similar overall qualitative behavior.
- Finally, in Section 5 we discuss implications for mechanistic interpretability and suggest compelling future work.

## 2 INCIDENTAL POLYSEMANTICITY FROM REGULARIZATION

In this section, as a first step, we show how polysemanticity can arise from a push for sparsity that is induced by  $l_1$  regularization term on the representations.

**Network and data** We consider a shallow nonlinear autoencoder similar to the setup described by Elhage et al. (2022). The model is a shallow nonlinear autoencoder with  $n$  features (inputs or outputs), a weight  $W \in \mathbb{R}^{n \times m}$  tying between the encoder and the decoder, and a single hidden layer of size  $m$  with  $l_1$  regularization of parameter  $\lambda$  on the activations. The network has a ReLU on the output layer with no biases, and is trained with the  $n$  standard basis vectors as data (so that

<sup>2</sup>Analogous phenomena are known under other names, such as “privileged basis”.

<sup>3</sup>If there is a three-way collision between  $i, j$  and  $k$ , that would count as three collisions between  $i$  and  $j$ ,  $i$  and  $k$ , and  $j$  and  $k$ .

the “features” are just individual input coordinates): that is, the input/output data pairs are  $(e_i, e_i)$  for  $i \in [n]$ , where  $e_i \in \mathbb{R}^n$  is the  $i^{\text{th}}$  basis vector. The shallow nonlinear autoencoder’s output is computed as  $y := \text{ReLU}(WW^T x)$ .

The main difference compared to the shallow nonlinear autoencoder from Elhage et al. (2022) is the addition of  $l_1$  regularization. The role of the  $l_1$  regularization is to push for sparsity in the activations and therefore induce a winner-take-all dynamic. As a result, our model facilitates precise and analytical study of incidental polysemanticity in particular. However, we believe our observations generalize further (see Section 5 for more on this); for instance, even if  $l_1$  regularization is not widely used in practice, recent work has also shown that other factors such as noisy data can implicitly induce sparsity-favoring regularization (Bricken et al., 2023). We make the following assumptions on parameter values:

- the weights  $W_{ik}$  are initialized to i.i.d. normals of mean 0 and standard deviation  $\Theta(1/\sqrt{m})$  so that the encodings  $W_i \in \mathbb{R}^m$  start out with constant length.
- $m \geq n$ , such that, evidently, polysemanticity is not necessary in this setting.
- $\lambda \leq 1/\sqrt{m}$  such that  $l_1$  regularization does not impose total and degenerate sparsity on weights.

**Possible solutions** Let  $W_i \in \mathbb{R}^m$  be the  $i^{\text{th}}$  row of  $W$ , which describes  $i^{\text{th}}$  feature is encoded in the hidden layer. When the input is  $e_i$ , the output of the model can then be written as

$$(\text{ReLU}(W_1 \cdot W_i), \dots, \text{ReLU}(W_n \cdot W_i)),$$

To achieve perfect reconstruction of  $e_i$ , we must have  $\|W_i\|^2 = 1^4$  and  $W_i \cdot W_j \leq 0$  for  $j \neq i$ . Letting  $f_k \in \mathbb{R}^m$  denote the  $k^{\text{th}}$  basis vector in  $\mathbb{R}^m$ . There are both monosemantic and polysemantic solutions that satisfy these conditions:

- A monosemantic solution is to simply let  $W_i := f_i$ : the  $i^{\text{th}}$  hidden neuron represents the  $i^{\text{th}}$  feature.
- An example polysemantic solution is to have two features share the same neuron, with opposite signs. For example, for each  $i \in [n/2]$ , we could let  $W_{2i-1} := f_i$  and  $W_{2i} := -f_i$ . Such a setup satisfies the requisites as  $W_{2i-1} \cdot W_{2i} = f_i \cdot (-f_i) = -1 \leq 0$ .
- In general, we can have a mixture of the above solutions in an arbitrary order, whereby each neuron represents either 0, 1 or 2 features.

**Learning dynamics and loss** Let us consider total squared error loss  $\mathcal{L}$ , which can be written as

$$\sum_i \left( (1 - \|W_i\|^2)^2 + \sum_{j \neq i} \text{ReLU}(W_i \cdot W_j)^2 + \lambda \|W_i\|_1 \right).$$

The training dynamics are:

$$\begin{aligned} \frac{dW_i}{dt} &:= - \frac{\partial \mathcal{L}}{\partial W_i} \\ &= 4(1 - \|W_i\|^2) W_i \quad \text{(feature benefit)} \\ &\quad - 4 \sum_{j \neq i} \text{ReLU}(W_i \cdot W_j) W_j \quad \text{(interference)} \\ &\quad - \lambda \text{sign}(W_i) \quad \text{(regularization)} \end{aligned}$$

where  $t$  is the training time (which corresponds to the learning rate multiplied by the number of training steps). For simplicity, we’ll ignore the constants 4 going forward<sup>5</sup>.

<sup>4</sup>We use  $\|\cdot\|$  to denote Euclidean length ( $l_2$  norm), and  $\|\cdot\|_1$  to denote Manhattan length ( $l_1$  norm).

<sup>5</sup>This is equivalent to making  $\lambda$  four times larger and making training time four times slower.

The gradient can be decomposed into three intuitive “forces” acting on the encodings  $W_i$ : (1) “feature benefit”: encodings want to have unit length; (2) “interference”: different encodings avoid pointing in similar directions; (3) “regularization”: encodings aim to have small  $l_1$ -norm (which pushes all nonzero weights towards zero with equal strength).

**The winning neuron takes it all** Setting aside the interference force momentarily, we aim to devise out the mechanism and speed by which regularization will push towards sparsity in some encoding  $W_i$ . As the only forces are feature benefit and regularization, the other encodings  $W_j$  have no influence on  $W_i$ . Assuming  $\|W_i\| < 1$ , each weight  $W_{ik}$  is pushed up with strength  $(1 - \|W_i\|^2) W_{ik}$  by the feature benefit force and pushed down with strength  $\lambda \text{sign}(W_{ik})$  by the regularization force.

Crucially, the upwards push is *relative* to how large  $W_{ik}$  is, while the downwards push is *absolute*. This means that weights whose absolute value is above some threshold  $\theta$  will grow, while those below the threshold will shrink, creating a “rich get richer and poor get poorer” dynamic that will push for sparsity. This threshold is determined by

$$(1 - \|W_i\|^2)W_{ik} = \lambda \text{sign}(W_{ik}) \iff |W_{ik}| = \frac{\lambda}{1 - \|W_i\|^2}$$

By letting  $\theta := \frac{\lambda}{1 - \|W_i\|^2}$ , we have

$$\begin{aligned} \frac{d|W_{ik}|}{dt} &= \underbrace{(1 - \|W_i\|^2)|W_{ik}|}_{\text{feature benefit}} - \underbrace{\lambda \mathbb{1}[W_{ik} \neq 0]}_{\text{regularization}} \\ &= \begin{cases} \underbrace{(1 - \|W_i\|^2)}_{\text{constant in } k} \underbrace{(|W_{ik}| - \theta)}_{\text{distance from threshold}} & \text{if } W_{ik} \neq 0 \\ 0 & \text{otherwise.} \end{cases} \end{aligned}$$

We call this combination of feature benefit and regularization force the *sparsity* force. It uniformly stretches the gaps between (the absolute values of) different nonzero weights. Note that the threshold  $\theta$  is not fixed: as  $W_i$  gets sparser,  $\|W_i\|^2$  will get closer to 1, which increases the threshold and allows the elimination of larger and larger entries, until only one remains.

**How quickly does sparsification occur?** In order to determine the pace at which  $W_i$  sparsifies, we will look at the  $l_1$  norm  $\|W_i\|_1 = \sum_k |W_{ik}|$  as a proxy for how many nonzero coordinates are left. Since we have  $\|W_i\| \approx 1$  throughout, if  $W_i$  has  $m'$  nonzero values at any point in time, their typical value will be  $\pm 1/\sqrt{m'}$ . This in turn implies  $\|W_i\|_1 \approx m' \frac{1}{\sqrt{m'}} = \sqrt{m'}$ .

Since the sparsity force is proportional to  $1 - \|W_i\|^2$ , we seek to determine the range of values  $\|W_i\|$  may take over time. As  $\|W_i\|$  changes relatively slowly, we can achieve useful insights by assuming  $\frac{d\|W_i\|^2}{dt}$  is 0:

$$0 \approx \frac{d\|W_i\|^2}{dt} = 2 \frac{dW_i}{dt} \cdot W_i = 2 \left( \underbrace{\left( (1 - \|W_i\|^2) \|W_i\|^2 \right)}_{\text{from feature benefit}} - \underbrace{\lambda \|W_i\|_1}_{\text{from regularization}} \right),$$

which implies  $1 - \|W_i\|^2 \approx \frac{\lambda \|W_i\|_1}{\|W_i\|^2}$ . Plugging this back into  $\frac{d\|W_i\|_1}{dt} = \sum_k \frac{d|W_{ik}|}{dt}$  and using reasonable assumptions about the initial distribution of  $W_i$ , we prove (see Appendix B for details) that  $\|W_i\|_1$  decreases proportionally to  $1/\lambda t$  with training time  $t$ :

$$\|W_i(t)\|_1 = \begin{cases} \Theta(\sqrt{m}) & t \leq \frac{1}{\lambda\sqrt{m}} \\ \Theta\left(\frac{1}{\lambda t}\right) & \frac{1}{\lambda\sqrt{m}} \leq t \leq \frac{1}{\lambda} \\ \Theta(1) & t \geq \frac{1}{\lambda}. \end{cases}$$

Concretely, let us approximate the number  $m'$  of nonzero coordinates as  $\|W_i\|_1^2$ . Over the course of training,  $m'$  will start at  $m$ , decrease as  $1/(\lambda t)^2$ , then reach 1 at training time  $t = \Theta(1/\lambda)$ .

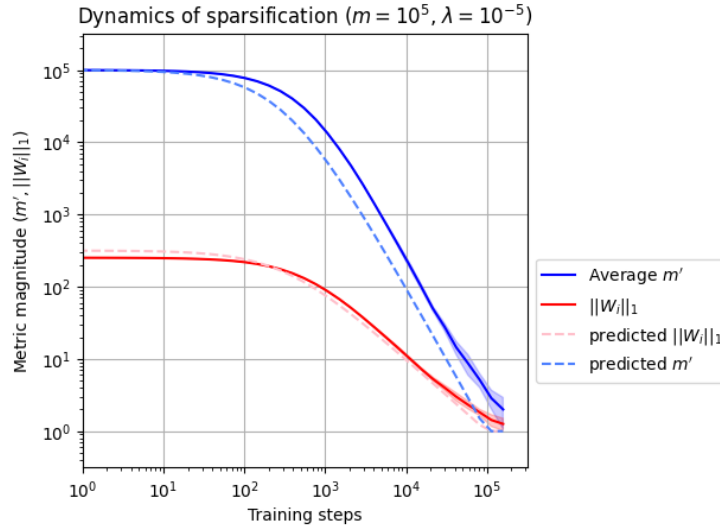


Figure 2: Number of non-zero coordinates  $m'$  in  $W_i$  and the value of  $\|W_i\|_1$  plotted with training steps. The simulation confirms the speed of sparsification hypothesis.

**Numerical simulations** In Figure 2 we compare our theoretical predictions for  $\|W_i\|_1$  and  $m'$  (if the constants hidden in  $\Theta(\cdot)$  are assumed to be 1) to their true values over training time when the interference force is turned off. The specific values of parameters are  $m := 10^5$  and  $\lambda := 10^{-5}$ , and the initial weights  $W_{ik}$  were generated as independent mean-0 normals with standard deviation  $0.9/\sqrt{m}$ .

## 2.1 INTERFERENCE ARBITERS COLLISIONS BETWEEN FEATURES

Resuming our consideration of the interference force in the gradient, we argue informally that the interference is initially weak if  $m \geq n$ , and only becomes significant later in training. In cases where two of the encodings  $W_i$  and  $W_j$  have a coordinate  $k$  such that  $W_{ik}$  and  $W_{jk}$  are both large and have the same sign, the larger of the two wins out due to the interference force.

**How strong is the interference?** First, observe that in the expression for the interference force on  $W_i$  is  $-\sum_{j \neq i} \text{ReLU}(W_i \cdot W_j)W_j$ , and each  $W_j$  contributes only if the angle it forms with  $W_i$  is less than  $90^\circ$ . Thus, the force will primarily be in the same direction as  $W_i$ , but opposite. We can get a good grasp on the strength of the force by measuring its component in the direction of  $W_i$  by taking an inner product with  $W_i$ .

We have  $(\sum_{j \neq i} \text{ReLU}(W_i \cdot W_j)W_j) \cdot W_i = \sum_{j \neq i} \text{ReLU}(W_i \cdot W_j)^2$ . Initially, each encoding is a vector of  $m$  i.i.d. normals of mean 0 and standard deviation  $\Theta(1/\sqrt{m})$ , so the distribution of the inner products  $W_i \cdot W_j$  is symmetric around 0 and also has standard deviation  $\Theta(1/\sqrt{m})$ . Therefore,  $\text{ReLU}(W_i \cdot W_j)^2$  has mean  $\Theta(1/m)$ , and the sum has mean  $\Theta(n/m)$ . As long as  $m \geq n$ , this is dominated by the feature benefit force: indeed, the same computation for the feature benefit gives

$$\left( (1 - \|W_i\|^2) W_i \right) \cdot W_i = (1 - \|W_i\|^2) \|W_i\|^2 = \Theta(1)$$

as long as  $\Omega(1) \leq \|W_i\|^2 \leq 1 - \Omega(1)$ .

Moreover, over time, the positive inner products  $W_i \cdot W_j > 0$  will tend to decrease exponentially. This is because the interference force on  $W_i$  includes the term  $-\text{ReLU}(W_i \cdot W_j)W_j$  and the interference force on  $W_j$  includes the term  $-\text{ReLU}(W_i \cdot W_j)W_i$ . Together, they affect  $W_i \cdot W_j$  as

$$(-\text{ReLU}(W_i \cdot W_j)W_j) \cdot W_j + (-\text{ReLU}(W_i \cdot W_j)W_i) \cdot W_i = -(W_i \cdot W_j) (\|W_i\|^2 + \|W_j\|^2) = -\Theta(W_i \cdot W_j)$$

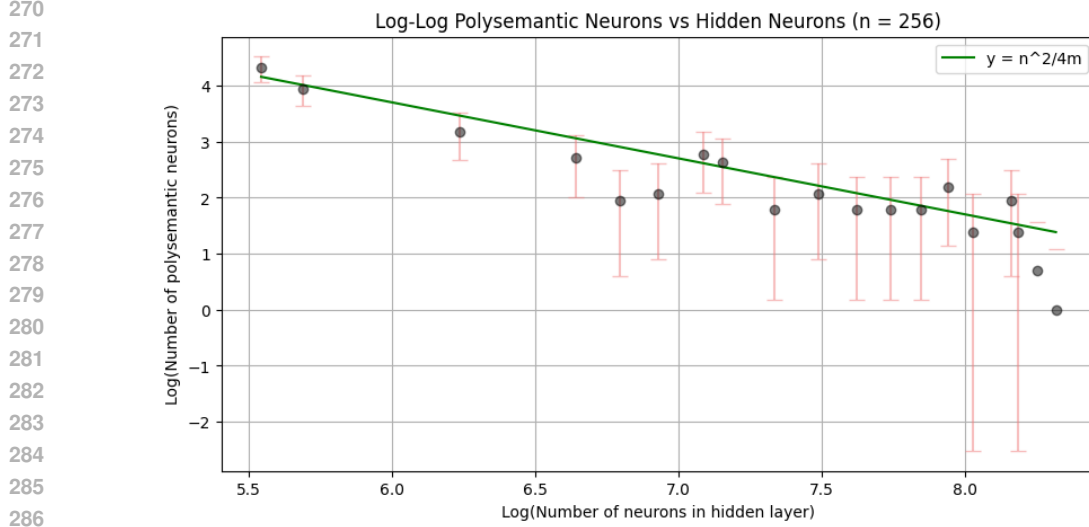


Figure 3: Number of polysemantic neurons against the number of neurons in the hidden layer for 16 different training runs of the non-linear autoencoder with  $n = 256$ .

as long as  $\|W_i\|^2, \|W_j\|^2 = \Theta(1)$ , which is the case at the start of training and persists throughout training.

**Benign and malign collisions** By contrast, the interference between two encodings  $W_i$  and  $W_j$  starts to matter significantly when one coordinate is affected much more strongly than the others (rather than affecting all coordinates proportionally, as with the feature benefit force). This is the case when  $W_i$  and  $W_j$  share only one nonzero coordinate: a single  $k$  such that  $W_{ik}, W_{jk} \neq 0$ . Under this scenario, the interference force  $-\text{ReLU}(W_i \cdot W_j)W_j$  only affects the coordinates of  $W_i$  that are nonzero in  $j$ , and likely is not strong enough to counter the  $l_1$ -regularization and revive coordinates of  $W_i$  that are currently zero. Therefore, only  $W_{ik}$  can be affected by this force.

When this happens, there are two cases:

- If  $W_{ik}$  and  $W_{jk}$  have opposite signs, we have  $W_i \cdot W_j = W_{ik}W_{jk} < 0$ . Due to the ReLU clipping the value to 0, there is no effect and we term this case a *benign collision*.
- If  $W_{ik}$  and  $W_{jk}$  have the same sign, we have  $W_i \cdot W_j = W_{ik}W_{jk} > 0$ , and both weights will be under pressure to shrink, with strength  $-W_{ik}W_{jk}^2$  and  $-W_{jk}^2W_{ik}$  respectively. Depending on the relative size of the weights, one or both of them will rapidly decay to 0. As a result,  $k^{\text{th}}$  neuron cannot represent the corresponding features and we term this case a *malign collision*.

Polysemanticity will happen when the largest<sup>6</sup> coordinates in encodings  $W_i$  and  $W_j$  get into a benign collision. This event occurs with probability

$$\underbrace{\frac{1}{m}}_{\text{largest weight in } W_i \text{ is also largest in } W_j} \times \underbrace{\frac{1}{2}}_{\text{opposite signs}} = \frac{1}{2m},$$

And therefore we should expect the number of polysemantic neurons to be, by the end, roughly:

$$\binom{n}{2} \times \frac{1}{2m} \sim \frac{n^2}{4m}$$

**Experiments:** Training networks on  $n \approx 256$  and  $m$  ranging from 256 to 4096 shows that this trend of  $\Theta\left(\frac{n^2}{m}\right)$  does hold, and the constant  $\frac{1}{4}$  seems to be fairly accurate as well (Figure 3).

<sup>6</sup>This would not necessarily be the largest weight at initialization, since there might be significant collisions with other encodings, but the largest weight at initialization is still the most likely to win the race all things considered.

### 3 ANOTHER INCENTIVE FOR SPARSITY: NOISE IN THE HIDDEN LAYER

In the toy model considered thus far, the encodings were incentivized to be sparse by an explicit  $l_1$  regularization term that was added into the loss. While this choice made the toy model simple to work with, this is not the most common reason why sparse representations occur in practice. In this section, loosely inspired by Blanc et al. (2020) and Bricken et al. (2023), we show that sparsity can arise when certain types of noise are present in the hidden layer.

#### 3.1 MODIFIED MODEL

We now consider a model identical to the previous one except that:

- the loss no longer contains the  $l_1$  regularization term  $\lambda \sum_i \|W_i\|_1$ ;
- every time the auto-encoder is run, noise from some noise distribution  $\mathcal{D}$  is added to each neuron in the hidden layer.

The output is computed as  $y := \text{ReLU}(W(W^\top x + \xi))$  for  $\xi \in \mathbb{R}^m$ , where each coordinate  $\xi_j$  is independently drawn from  $\mathcal{D}$ , and the loss for each input  $x$  is defined as

$$\mathcal{L} := \|y - x\|^2 = \|\text{ReLU}(W(W^\top x + \xi)) - x\|^2.$$

Throughout, we will assume that the noise distribution  $\mathcal{D}$  is symmetric around 0, has variance  $\sigma^2$ , and fourth central moment  $\mu_4$ . Note that this loss is fully rotationally symmetric in terms of the hidden layer’s space  $\mathbb{R}^m$ , except for possibly the noise  $\xi$ : if a rotation were applied right before the hidden layer and undone right after, the space would be invariant. In particular, if  $\mathcal{D}$  was a normal distribution  $\mathcal{N}(0, \sigma^2)$ , the rotational symmetry would be conserved and there would be no privileged directions for the encoding vectors to align to. In the remainder of this section, we show through both mathematical analysis and experiments that when the noise  $\xi_j$  has negative *excess kurtosis* (which includes many bounded distributions, such as bipolar noise or the uniform distribution over any interval), then the encodings are pushed towards sparsity.

#### 3.2 MATHEMATICAL ANALYSIS

Concretely, we compute the update after the  $t^{\text{th}}$  step of training, and show that the expected loss at the  $(t + 1)^{\text{th}}$  step has a term which involves both the fourth norms  $\|W_i\|_4$  of the encodings and the excess kurtosis of the noise distribution  $\mathcal{D}$ .

Since the computations are rather lengthy, we defer the details to Appendix C due to space constraints, but the summary is that:

- if  $\mathcal{D}$  is bipolar noise  $\pm\sigma$ , which has excess kurtosis  $-2$ , then this would push towards sparsity;
- if  $\mathcal{D}$  is normal noise  $\mathcal{N}(0, \sigma^2)$ , which has excess kurtosis 0, then this will not push towards sparsity (and indeed this would maintain the rotational symmetry of the hidden space  $\mathbb{R}^m$ , and sparsity is not rotationally symmetric).

## 4 COMPARING $l_1$ REGULARIZATION AND NOISE

In this section, we compare the ways that  $l_1$  regularization and noise induce sparsity and polysemanticity through various experiments. In Figure 4 we train autoencoders bipolar and normal noise of various intensities and plot the average fourth norms  $\|W_i\|_4^4$  of the encodings as a proxy for how sparse they are. We observe that as expected,

- bipolar noise pushes encodings towards sparsity, and the higher the standard deviation  $\sigma$  is, the faster this is;
- on the other hand, in the presence of *normal* noise, there is no observable effect on sparsity, and it only makes the fourth norms oscillate.

378  
379  
380  
381  
382  
383  
384  
385  
386  
387  
388  
389  
390  
391  
392  
393  
394  
395  
396  
397  
398  
399  
400  
401  
402  
403  
404  
405  
406  
407  
408  
409  
410  
411  
412  
413  
414  
415  
416  
417  
418  
419  
420  
421  
422  
423  
424  
425  
426  
427  
428  
429  
430  
431

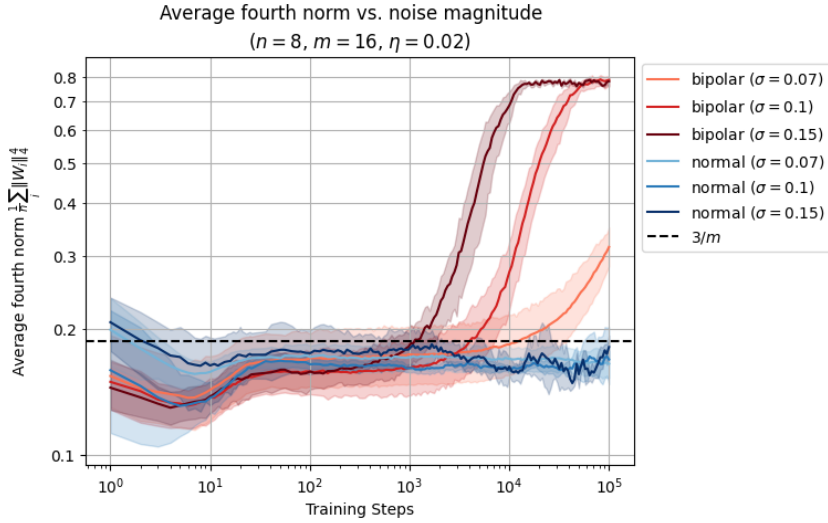


Figure 4: Sparsification process under bipolar and normal noise of various magnitudes. The line  $3/m$  is added in as a reference since for large  $m$  it is asymptotic to the fourth norm of a random unit vector.

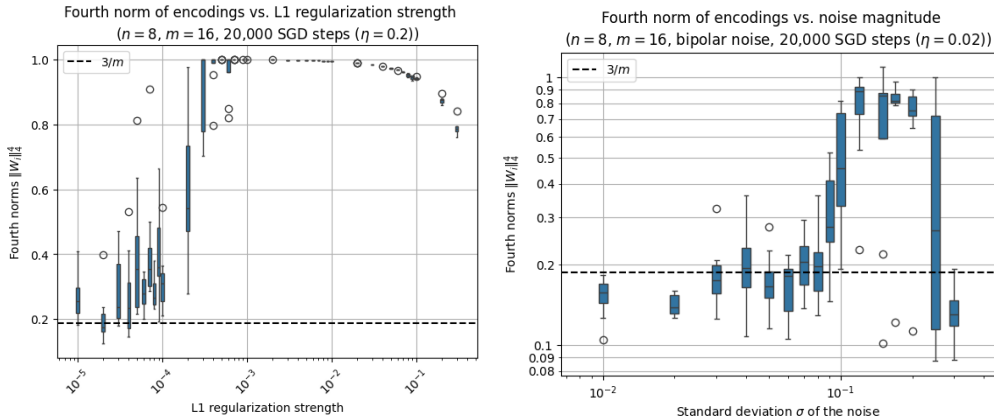


Figure 5: Final fourth norms under  $l_1$  regularization and bipolar noises of various magnitudes. The line  $3/m$  is the asymptotical value of the fourth norm of a random unit vector.

In Figure 5, we dig deeper into the effect of the regularization coefficient  $\lambda$  (Section 4) and the standard deviation  $\sigma$  (Section 4) on the sparsity after a fixed number of steps. We confirm that regularization and noise of small magnitudes have almost no effect on sparsity and the effect generally grows with magnitude, but the effect from  $\sigma$  is much stronger since it appears as a 4<sup>th</sup> power in the implicit regularization, whereas  $l_1$  regularization is linear in  $\lambda$ . When the regularization and noise get extremely large, we see a drop in the fourth norms due to an overall drop in the magnitudes  $\|W_i\|_2$  of the encodings, but the reasons differ slightly:

- when  $\lambda$  is very high, the  $l_1$  regularization pushes down on all coordinates of each encoding  $W_i$  strongly, and once that threshold becomes large enough, the feature benefit force is no longer strong enough to counteract it, even if the encoding  $W_i$  is perfectly sparse;
- when  $\sigma$  is very high, the direct corruption that the noises induces on the pre-ReLU outputs becomes significant, so the lengths  $\|W_i\|_2$  of the encodings are incentivized to shorten.

In Figure 6, we consider a the training dynamics of a typical instance under bipolar noise. In Section 4, we separately plot the fourth-norm of each encoding  $W_i$ , and observe that even though most of the



432  
433  
434  
435  
436  
437  
438  
439  
440  
441  
442  
443  
444  
445  
446  
447  
448  
449  
450  
451  
452  
453  
454  
455  
456  
457  
458  
459  
460  
461  
462  
463  
464  
465  
466  
467  
468  
469  
470  
471  
472  
473  
474  
475  
476  
477  
478  
479  
480  
481  
482  
483  
484  
485

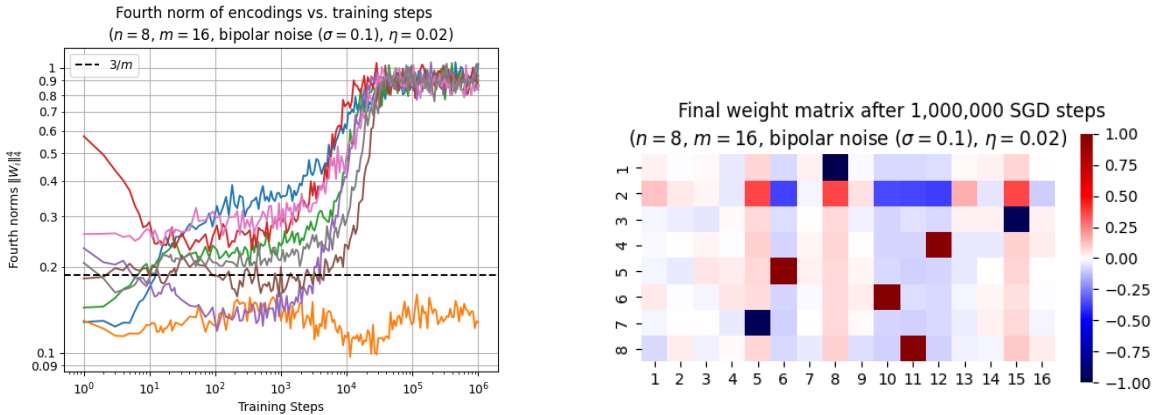


Figure 6: Sparsification process for a specific instance at  $\sigma = 0.01$  of bipolar noise, and the final weight matrix after 1M training steps.

encodings reach almost perfect sparsity (indicated by  $\|W_i\|_4^4 \approx 1$ ), the encoding corresponding to the orange curve seems to be stuck below  $\|W_i\|_4^4 = 0.2$ . This can be explained by looking at Section 4, which visualizes the corresponding final weight matrix  $W$ . The second encoding row  $W_2$  has significant weights in the 7 coordinates that were chosen by the other encodings, and that these weights all have comparable absolute values. What’s happening is a fascinating interplay between the interference and the push for sparsity.

- On the one hand, the push for sparsity should incentivize  $W_2$  to “pick” one of these 7 coordinates and increase its absolute value at the detriment of the other 6. Indeed, in all cases, the sign of  $W_{2j}$  is the opposite of the sign of  $W_{ij}$  for the encoding  $i$  which maximizes  $|W_{ij}|$ , so naively, this shouldn’t cause any interference.
- But the smaller weights in the matrix  $W$  provide a hint to what is actually happening: in each column  $j$  for which there is some  $i$  with  $|W_{ij}| \approx 1$ , the other encodings  $W_{i'}$  have a small but non-negligible weight with the opposite sign. This is detrimental in terms of the implicit regularization term, but it ensures that the dot product  $W_{i'} \cdot W_i$  remains negative (or at least small) even after a small amount of noise is applied to the hidden layer on input  $e_{i'}$ . If  $W_2$  were to choose one of these coordinates  $j$ , then there would be no such strategy available: indeed, if  $W_i$  and  $W_2$  were equal the basis vectors  $e_j$  and its opposite  $-e_j$ , then one of  $W_{i'} \cdot W_i$  or  $W_{i'} \cdot W_2$  must be nonnegative, and changing the value of  $W_{i'j}$  in either direction would only make things worse. So  $W_2$  is kept from applying this strategy, and is instead forced to compromise between all 7 coordinates in order to keep interference at a minimum.

This phenomenon is strikingly different from the type of polysemanticity that we studied in the previous sections. It also explains why the fourth norms were not quite approaching 1 in Figure 4.

## 5 DISCUSSION AND FUTURE WORK

Until now, the mechanistic interpretability literature has mostly studied polysemanticity in settings where the encoding space has no privileged basis: the space can be arbitrarily rotated without changing the dynamics, and in particular the corresponding layer doesn’t have non-linearities or any regularization other than  $l_2$ . In such settings, the features can be represented arbitrarily in the encoding space, and we only observe superposition (non-orthogonal encodings) when there are more features than dimensions.

When there is no privileged basis, it is always technically feasible to get rid of superposition by simply increasing the number of neurons so that it matches the number of features. Eliminating polysemanticity that is due to non-task factors could require completely different tools, and seems

486 particularly challenging given that (as we saw in Figure 6), that kind of polysemanticity can happen  
487 for a wide variety of sometimes surprisingly hard-to-predict incidental reasons.

488  
489 In particular, it is much less realistic to do away with the kind of incidental polysemanticity that we  
490 demonstrate in Section 2 by simply increasing the number of hidden neurons, since we saw that it  
491 can happen until the number of hidden neurons is roughly equal to the number of features *squared*.  
492 For instance, here is one possible way one might get rid of incidental polysemanticity in a neuron  
493 that currently represents two features  $i$  and  $j$ : Duplicate that neuron, divide its outgoing weights by 2  
494 (so that this doesn't affect downstream layers), add a small amount of noise to the incoming weights  
495 of each copy, then run gradient descent for a few more steps. This might cause the copies to diverge  
496 away from each other, with one of the copies eventually taking full ownership of feature  $i$  while the  
497 other copy takes full ownership of feature  $j$ .

498 In addition, it would be interesting to find ways to distinguish incidental polysemanticity from  
499 necessary polysemanticity in practice. Can we distinguish them based only on the final, trained state  
500 of the model, or do we need to know more about what happened during training? Is "most" of the  
501 polysemanticity in real-world neural networks necessary or incidental? How does this depend on the  
502 architecture and the data?

503 In this paper, we presented a new challenge for mechanistic interpretability beyond traditional super-  
504 position, demonstrating that polysemanticity can be an inherent outcome even in overparameterized  
505 networks. Since polysemantic neurons may emerge due to incidental factors rather than task-related  
506 constraints, this work opens up the possibility to understand complex feature representations in  
507 deep neural networks, where training dynamics decrease our ability to interpret and predict network  
508 behavior.

509  
510  
511  
512  
513  
514  
515  
516  
517  
518  
519  
520  
521  
522  
523  
524  
525  
526  
527  
528  
529  
530  
531  
532  
533  
534  
535  
536  
537  
538  
539

## REFERENCES

- 540  
541  
542 Wael F Asaad, Gregor Rainer, and Earl K Miller. Neural activity in the primate prefrontal cortex  
543 during associative learning. *Neuron*, 21(6):1399–1407, 1998.
- 544 Omri Barak, Mattia Rigotti, and Stefano Fusi. The sparseness of mixed selectivity neurons controls  
545 the generalization–discrimination trade-off. *Journal of Neuroscience*, 33(9):3844–3856, 2013.
- 546  
547 Guy Blanc, Neha Gupta, Gregory Valiant, and Paul Valiant. Implicit regularization for deep neural  
548 networks driven by an ornstein-uhlenbeck like process, 2020.
- 549 Trenton Bricken, Rylan Schaeffer, Bruno Olshausen, and Gabriel Kreiman. Emergence of sparse  
550 representations from noise. In *International Conference on Machine Learning*. PMLR, 2023.
- 551  
552 Nelson Elhage, Tristan Hume, Catherine Olsson, Nicholas Schiefer, Tom Henighan, Shauna  
553 Kravec, Zac Hatfield-Dodds, Robert Lasenby, Dawn Drain, Carol Chen, Roger Grosse,  
554 Sam McCandlish, Jared Kaplan, Dario Amodei, Martin Wattenberg, and Christopher Olah.  
555 Toy models of superposition. *Transformer Circuits Thread*, 2022. [https://transformer-](https://transformer-circuits.pub/2022/toy_model/index.html)  
556 [circuits.pub/2022/toy\\_model/index.html](https://transformer-circuits.pub/2022/toy_model/index.html).
- 557 Stefano Fusi, Earl K Miller, and Mattia Rigotti. Why neurons mix: high dimensionality for higher  
558 cognition. *Current opinion in neurobiology*, 37:66–74, 2016.
- 559 Dan Hendrycks, Mantas Mazeika, and Thomas Woodside. An overview of catastrophic ai risks.  
560 *arXiv preprint arXiv:2306.12001*, 2023.
- 561  
562 W Jeffrey Johnston, Stephanie E Palmer, and David J Freedman. Nonlinear mixed selectivity supports  
563 reliable neural computation. *PLoS computational biology*, 16(2):e1007544, 2020.
- 564 Grace W Lindsay, Mattia Rigotti, Melissa R Warden, Earl K Miller, and Stefano Fusi. Hebbian  
565 learning in a random network captures selectivity properties of the prefrontal cortex. *Journal of*  
566 *Neuroscience*, 37(45):11021–11036, 2017.
- 567  
568 Farshad A Mansouri, Kenji Matsumoto, and Keiji Tanaka. Prefrontal cell activities related to monkeys’  
569 success and failure in adapting to rule changes in a wisconsin card sorting test analog. *Journal of*  
570 *Neuroscience*, 26(10):2745–2756, 2006.
- 571 Richard Ngo, Lawrence Chan, and Sören Mindermann. The alignment problem from a deep learning  
572 perspective. *arXiv preprint arXiv:2209.00626*, 2022.
- 573  
574 Chris Olah, Alexander Mordvintsev, and Ludwig Schubert. Feature visualization. *Distill*, 2017. doi:  
575 10.23915/distill.00007. <https://distill.pub/2017/feature-visualization>.
- 576  
577 Chris Olah, Nick Cammarata, Ludwig Schubert, Gabriel Goh, Michael Petrov, and Shan Carter.  
578 Zoom in: An introduction to circuits. *Distill*, 2020. doi: 10.23915/distill.00024.001.  
<https://distill.pub/2020/circuits/zoom-in>.
- 579  
580 Matthias Oster, Rodney Douglas, and Shih-Chii Liu. Computation with Spikes in a Winner-Take-All  
581 Network. *Neural Computation*, 21(9):2437–2465, 09 2009. ISSN 0899-7667. doi: 10.1162/neco.  
582 2009.07-08-829. URL <https://doi.org/10.1162/neco.2009.07-08-829>.
- 583  
584 Aishwarya Parthasarathy, Roger Herikstad, Jit Hon Bong, Felipe Salvador Medina, Camilo Libedin-  
585 sky, and Shih-Cheng Yen. Mixed selectivity morphs population codes in prefrontal cortex. *Nature*  
*neuroscience*, 20(12):1770–1779, 2017.
- 586  
587 David Raposo, Matthew T Kaufman, and Anne K Churchland. A category-free neural population  
588 supports evolving demands during decision-making. *Nature neuroscience*, 17(12):1784–1792,  
2014.
- 589  
590 Mattia Rigotti, Omri Barak, Melissa R Warden, Xiao-Jing Wang, Nathaniel D Daw, Earl K Miller,  
591 and Stefano Fusi. The importance of mixed selectivity in complex cognitive tasks. *Nature*, 497  
592 (7451):585–590, 2013.
- 593  
Melissa R Warden and Earl K Miller. The representation of multiple objects in prefrontal neuronal  
delay activity. *Cerebral cortex*, 17(suppl\_1):i41–i50, 2007.

594 Carey Y Zhang, Tyson Aflalo, Boris Revechkis, Emily R Rosario, Debra Ouellette, Nader Pouratian,  
595 and Richard A Andersen. Partially mixed selectivity in human posterior parietal association cortex.  
596 *Neuron*, 95(3):697–708, 2017.  
597

598  
599  
600  
601  
602  
603  
604  
605  
606  
607  
608  
609  
610  
611  
612  
613  
614  
615  
616  
617  
618  
619  
620  
621  
622  
623  
624  
625  
626  
627  
628  
629  
630  
631  
632  
633  
634  
635  
636  
637  
638  
639  
640  
641  
642  
643  
644  
645  
646  
647

## 648 A GENERALITY OF THE MODEL

649  
650  
651 We chose the toy model in Section 2 to be as simple as possible (and to match Elhage et al. (2022) as  
652 closely as possible) while still exhibiting incidental polysemanticity. Nevertheless, in this section, we  
653 want to point out that some of these choices are actually without loss of (much) generality.

654  
655  
656 **Tied weights** In our model, the encoding and decoding matrices are tied together (i.e. the encoding  
657 matrix  $W^T$  is forced to be the transpose of the decoding matrix  $W$ ). This assumption makes sense  
658 because even if they were kept independent and initialized to different values, they would naturally  
659 acquire similar values over time because of the learning dynamics. Indeed, the  $i^{\text{th}}$  column of the  
660 encoding matrix and the  $i^{\text{th}}$  row of the decoding matrix “reinforce each other” through the feature  
661 benefit force until they have an inner product of 1, and as long as they start out small or if there is  
662 some weight decay, they would end up almost identical by the end of training.

663  
664 **Basis vectors as inputs** If the input features are not the canonical basis vectors but are still  
665 orthogonal (and the outputs are still basis vectors), then we could apply a fixed linear transformation  
666 to the encoding matrix and recover the same training dynamics. And in general it makes sense to  
667 consider orthogonal input features, because when the features themselves are not orthogonal (or  
668 at least approximately orthogonal), the question of what polysemanticity even is becomes quite  
669 confused.

## 670 B RIGOROUS ANALYSIS OF THE SPEED OF SPARSIFICATION UNDER $l_1$ 671 REGULARIZATION

672  
673 For  $m' := \#\{k \mid W_{ik} \neq 0\}$ , one can write that

$$\begin{aligned}
 674 \quad -\frac{d\|W_i\|_1}{dt} &= \underbrace{\lambda m'}_{\text{regularization}} - \underbrace{(1 - \|W_i\|^2) \|W_i\|_1}_{\text{feature benefit}} \\
 675 &= \frac{\lambda}{\|W_i\|^2} (m' \|W_i\|^2 - \|W_i\|_1^2) && \text{(by balance condition)} \\
 676 &= \frac{\lambda(m')^2}{\|W_i\|^2} \left( \frac{\|W_i\|^2}{m'} - \left( \frac{\|W_i\|_1}{m'} \right)^2 \right) \\
 677 &= \frac{\lambda(m')^2}{\|W_i\|^2} \times \underbrace{\frac{\sum_{k:W_{ik} \neq 0} \left( \underbrace{|W_{ik}| - \frac{\|W_i\|_1}{m'}}_{\text{“deviation from mean”}} \right)^2}{m'}}_{\text{“sample variance over nonzero weights”}},
 \end{aligned}$$

678  
679 where the last inequality is essentially the identity

$$680 \quad \mathbb{E}[\mathbf{X}^2] - \mathbb{E}[\mathbf{X}]^2 = \text{Var}[\mathbf{X}]$$

681  
682 where the random variable  $\mathbf{X}$  is drawn by picking a  $k$  at uniformly at random in  $\{k \mid W_{ik} \neq 0\}$   
683 and outputting  $|W_{ik}|$ .

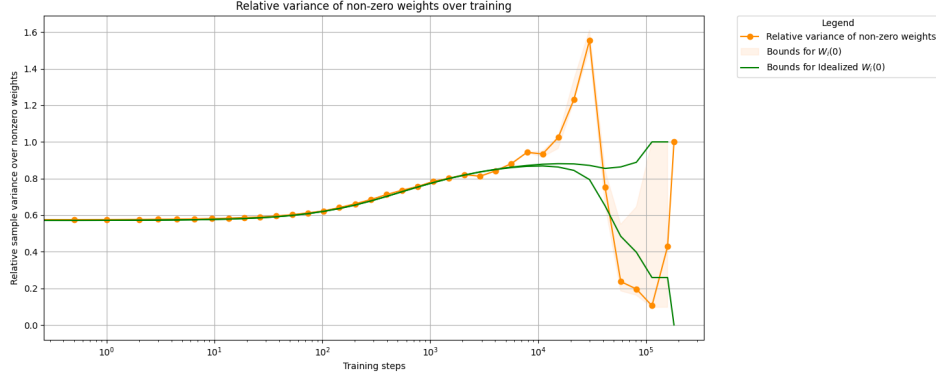


Figure 7: We plot the relative variance over time in the numerical simulation, showing that these lower and upper values for  $W_i(0)$  itself (in red) and for an idealized version of  $W_i(0)$  that hits regular percentiles (in pink, dashed).

If  $\mathbf{X}$ 's relative variance  $\frac{\text{Var}[\mathbf{X}]}{\mathbb{E}[\mathbf{X}]^2}$  is a constant, then

$$\begin{aligned}
 -\frac{d\|W_i\|_1}{dt} &= \frac{\lambda(m')^2}{\|W_i\|^2} \text{Var}[\mathbf{X}] \\
 &= \frac{\lambda(m')^2}{\|W_i\|^2} \Theta(\mathbb{E}[\mathbf{X}]^2) \\
 &= \Theta\left(\frac{\lambda}{\|W_i\|^2} \|W_i\|_1^2\right) \\
 &= \Theta(\lambda \|W_i\|_1^2), \quad (\text{assuming } \|W_i\|^2 = \Theta(1))
 \end{aligned}$$

or if we define  $w := \frac{1}{\|W_i\|_1}$  (which is a proxy for the “typical nonzero weight”, and is  $\approx \theta$  when  $\|W_i\|^2 \approx 1$ ), this becomes

$$\frac{dw}{dt} = \Theta(\lambda),$$

so  $w(t) = w(0) + \Theta(\lambda t)$  and

$$\|W_i(t)\|_1 = \frac{1}{\Theta(w(0) + \lambda t)} = \frac{1}{\Theta\left(\frac{1}{\sqrt{m}} + \lambda t\right)}$$

with high probability in  $m$ .

Empirically, the relative variance is indeed a constant not too far from 1 (see Figure 7). But why is that?

Suppose that currently  $W_{i1} \geq W_{i2} \geq \dots \geq W_{im} \geq 0$ , and let's look at the relative difference between the biggest weight  $W_{i1}$  and some other weight  $W_{ik} > 0$ , i.e.

$$\gamma_k := \frac{W_{i1} - W_{ik}}{W_{i1}} = 1 - \frac{W_{ik}}{W_{i1}}.$$

Using logarithmic derivatives, we have

$$\frac{d\gamma_k}{dt} = -\frac{d(W_{ik}/W_{i1})}{dt} = -\frac{W_{ik}}{W_{i1}} \left( \frac{dW_{ik}/dt}{W_{ik}} - \frac{dW_{i1}/dt}{W_{i1}} \right)$$

Since feature benefit is a relative force, it contributes nothing to the difference of the relative derivatives of  $W_{ik}$  and  $W_{i1}$ , so we just have the contribution from regularization

$$\begin{aligned} \frac{d\gamma_k}{dt} &= -\frac{W_{ik}}{W_{i1}} \left( \frac{-\lambda}{W_{ik}} - \frac{-\lambda}{W_{i1}} \right) \\ &= \frac{\lambda W_{ik}}{W_{i1}} \left( \frac{1}{W_{ik}} - \frac{1}{W_{i1}} \right) \\ &= \frac{\lambda}{W_{i1}} \left( 1 - \frac{W_{ik}}{W_{i1}} \right) \\ &= \frac{\lambda}{W_{i1}} \gamma_k. \end{aligned}$$

Note that this differential equation doesn't involve  $W_{ik}$  at all! This means that there is a single function  $\gamma(t)$  defined by

$$\begin{cases} \gamma(0) = 1 \\ \frac{d\gamma}{dt}(t) = \frac{\lambda}{W_{i1}(t)} \gamma(t) \end{cases}$$

such that for all  $k$ , as long as  $W_{ik}(t) > 0$ ,

$$\begin{aligned} 1 - \frac{W_{ik}(t)}{W_{i1}(t)} &= \gamma(t) \left( 1 - \frac{W_{ik}(0)}{W_{i1}(0)} \right) \\ \Rightarrow W_{ik}(t) &= \underbrace{W_{i1}(t)}_{\text{doesn't depend on } k} (1 - \gamma(t)) \\ &\quad + \underbrace{\frac{\gamma(t)W_{i1}(t)}{W_{i1}(0)}}_{\text{doesn't depend on } k} W_{ik}(0). \end{aligned}$$

In other words, the relative spacing of the nonzero weights never change: their change between times 0 and  $t$  is a single affine transformation.

Since the relative variance is scaling-invariant, we can think of this affine transformation as a simple translation. The value of the relative variance of the remaining nonzero weights  $W_{i1}(t), \dots, W_{im'}(t)$  at some point in time must be of the following form:

- take the initial values  $W_{i1}(0), \dots, W_{im'}(0)$ ,
- translate them left by some amount which leaves  $m'$  weights positive,
- drop the values that have become  $\leq 0$ ,
- then compute the relative variance of what's left.

In particular, the relative variance when  $m'$  weights are left must lie between the relative variance of

$$(W_{i1}(0) - W_{i(m'+1)}(0), \dots, W_{im'}(0) - W_{i(m'+1)}(0))$$

and the relative variance of

$$(W_{i1}(0) - W_{im'}(0), W_{i2}(0) - W_{im'}(0), \dots, 0)$$

(since these extremes have the same variance but the latter has a smaller mean).

These relative variances are functions of  $m'$  and the initial value of  $W_i$  only, and (when  $W_i$  is made of mean-0 normals) they will be  $\Theta(1)$  with high probability in  $m'$ . See the plot (see Figure 7) for a depiction of the lower and upper values for  $W_i(0)$  itself (shown in red), and also for an idealized version of  $W_i(0)$  that hits regular percentiles (in pink, dashed). The orange curve lies within the red curves, and that the red and pink curves only start to diverge significantly at later time steps when  $m'$  is smaller, for reasons detailed above.

## C GRADIENT AND LOSS COMPUTATIONS UNDER NOISE

### C.1 GRADIENT AT THE PREVIOUS STEP

To simplify analysis, we assume that after  $t$  steps of training, the representations are fully learned and there is no interference. More precisely,

1. each encoding  $W_i$  has norm  $\|W_i\|_2 = 1$ ;
2. dot product  $W_i \cdot W_{i'}$  between pairs of different encodings ( $i \neq i'$ ) is sufficiently negative the noise  $\xi$  will not “accidentally turn on” the ReLU’s at output coordinate  $i'$  when the input is the  $i^{\text{th}}$  basis vector:  $(W_i + \xi) \cdot W_{i'}$  with high probability.

Let’s compute the gradient at the  $t^{\text{th}}$  step. To make the math easier to follow, let’s temporarily rename the encoding matrix to  $W^e$  and the decoding matrix to  $W^d$ , even though these are the same matrix  $W$ . For an input  $x$ , let’s consider the values of the hidden layer  $h$ , the output  $y$ , the error  $\epsilon$  and the loss  $\mathcal{L}$ :

$$\begin{aligned} h &:= (W^e)^\top x + \xi && \in \mathbb{R}^m \\ y &:= \text{ReLU}(W^d h) && \in \mathbb{R}^n \\ \epsilon &:= y - x && \in \mathbb{R}^n \\ \mathcal{L} &:= \|\epsilon\|^2 && \in \mathbb{R}. \end{aligned}$$

Let  $x$  is the  $i^{\text{th}}$  basis vector  $e_i$ . Then

- $h = (W^e)^\top e_i + \xi = W_i^e + \xi$ ;
- the output  $y$  is 0 everywhere (with ReLUs turned off) except for the  $i^{\text{th}}$  coordinate, which is  $y_i = W_i^d \cdot W_i^e + W_i^d \cdot \xi = 1 + W_i^d \cdot \xi$ , so  $\epsilon_i = W_i^d \cdot \xi$ ;
- $\frac{\partial \mathcal{L}}{\partial o_i} = 2\epsilon_i$  so  $\frac{\partial \mathcal{L}}{\partial W_i^d} = \frac{\partial \mathcal{L}}{\partial o_i} \frac{\partial o_i}{\partial W_i^d} = 2\epsilon_i h = 2(W_i^d \cdot \xi)(W_i^e + \xi)$ ;
- $\frac{\partial \mathcal{L}}{\partial h} = \frac{\partial \mathcal{L}}{\partial o_i} \frac{\partial o_i}{\partial h} = 2(W_i^d \cdot \xi) W_i^d$  so  $\frac{\partial \mathcal{L}}{\partial W_i^e} = \frac{\partial \mathcal{L}}{\partial h} \frac{\partial h}{\partial W_i^e} = \frac{\partial \mathcal{L}}{\partial h} I_n = 2(W_i^d \cdot \xi) W_i^d$ .

Overall, recalling that  $W^e = W^d = W$ , we have  $\frac{\partial \mathcal{L}}{\partial W_i} = 2(W_i \cdot \xi)(2W_i + \xi)$ , and all other gradients are zero on this input. We will see that the part which will push for sparsity is  $2(W_i \cdot \xi)\xi$ ; everything else will either cancel out, almost cancel out, or give rotationally symmetric terms.

By gradient descent, we have  $W^{(t+1)} := W^{(t)} - \eta \frac{\partial \mathcal{L}}{\partial W}$ , so that for each  $i \in [n]$ ,

$$W_i^{(t+1)} = W_i^{(t)} - 2\eta(W_i \cdot \xi)(2W_i + \xi).$$

Expected loss at the next step At the next step, we get error  $W_i^{(t+1)} \cdot (W_i^{(t+1)} + \xi') - 1 = \left\| W_i^{(t+1)} \right\|^2 - 1 + W_i^{(t+1)} \cdot \xi'$ , where  $\xi'$  is the new noise, so the expected loss on input  $e_i$  is

$$\begin{aligned} & \mathbb{E} \left[ \left( \left\| W_i^{(t+1)} \right\|^2 - 1 + W_i^{(t+1)} \cdot \xi' \right)^2 \right] \\ &= \mathbb{E} \left[ \left( \left\| W_i^{(t+1)} \right\|^2 - 1 \right)^2 \right] + \mathbb{E} \left[ \left( W_i^{(t+1)} \cdot \xi' \right)^2 \right] \\ & \quad + 2 \mathbb{E} \left[ \left( \left\| W_i^{(t+1)} \right\|^2 - 1 \right) W_i^{(t+1)} \cdot \underbrace{\xi'}_{\mathbb{E}[\cdot]=0} \right] \\ &= \underbrace{\mathbb{E} \left[ \left( \left\| W_i^{(t+1)} \right\|^2 - 1 \right)^2 \right]}_{\text{involves } \xi \text{ only}} + \underbrace{\mathbb{E} \left[ \left( W_i^{(t+1)} \cdot \xi' \right)^2 \right]}_{\text{involves } \xi \text{ and } \xi'}, \end{aligned}$$



and we can simplify the second part to

$$\mathbb{E}\left[\left(W_i^{(t+1)} \cdot \xi'\right)^2\right] = \sigma^2 \mathbb{E}\left[\left\|W_i^{(t+1)}\right\|^2\right].$$

Since we've reduced both terms to quantities that involve only  $\left\|W_i^{(t+1)}\right\|^2$ , let's study it closer:

$$\begin{aligned} \left\|W_i^{(t+1)}\right\|^2 &= \left\|W_i - 2\eta(W_i \cdot \xi)(2W_i + \xi)\right\|^2 \\ &= \left\|W_i\right\|^2 - 4\eta(W_i \cdot \xi)\left(2\left\|W_i\right\|^2 + (W_i \cdot \xi)\right) \\ &\quad + 4\eta^2(W_i \cdot \xi)^2\left(4\left\|W_i\right\|^2 + 4(W_i \cdot \xi) + \left\|\xi\right\|^2\right) \\ &= 1 - 4\eta(W_i \cdot \xi)(2 + (W_i \cdot \xi)) \\ &\quad + 4\eta^2(W_i \cdot \xi)^2\left(4 + 4(W_i \cdot \xi) + \left\|\xi\right\|^2\right) \end{aligned}$$

First, let's deal with the part which involves the new noise  $\xi'$ . Because the noise distribution  $\mathcal{D}$  is symmetric around 0, we have  $\mathbb{E}[(W_i \cdot \xi)] = \mathbb{E}[(W_i \cdot \xi)^3] = 0$ , so

$$\begin{aligned} \mathbb{E}\left[\left\|W_i^{(t+1)}\right\|^2\right] \\ = 1 - 4\eta(1 - 4\eta) \mathbb{E}\left[(W_i \cdot \xi)^2\right] + 4\eta^2 \mathbb{E}\left[(W_i \cdot \xi)^2 \left\|\xi\right\|^2\right] \end{aligned}$$

and  $\mathbb{E}\left[(W_i \cdot \xi)^2\right] = \sigma^2 \left\|W_i\right\|^2 = \sigma^2$ , while

$$\begin{aligned} \mathbb{E}\left[(W_i \cdot \xi)^2 \left\|\xi\right\|^2\right] &= \mathbb{E}\left[\left(\sum W_{ij} \xi_j\right)^2 \sum \xi_j^2\right] \\ &= \mathbb{E}\left[\left(\sum W_{ij}^2 \xi_j^2\right) \sum \xi_j^2\right] \\ &= \left\|W_i\right\|^2 (\mu_4 + (m-1)\sigma^4) \end{aligned}$$

so the part of the expected loss involving both  $\xi$  and  $\xi'$  is

$$\sigma^2(1 - 4\eta(1 - 4\eta)\sigma^2 \pm 4\eta^2(\mu_4 + (m-1)\sigma^4)),$$

which is constant and therefore will not push  $W_i$  towards or away from sparsity.

Let's now move to the more interesting part, the error that involves only the old noise  $\xi$ . We have

$$\left\|W_i^{(t+1)}\right\|^2 - 1 = -4\eta(2(W_i \cdot \xi) + \eta(W_i \cdot \xi)^2) \pm O(\eta^2),$$

so

$$\begin{aligned} \mathbb{E}\left[\left(\left\|W_i^{(t+1)}\right\|^2 - 1\right)^2\right] \\ = 16\eta^2 \mathbb{E}\left[4(W_i \cdot \xi)^2 + 4(W_i \cdot \xi)^3 + (W_i \cdot \xi)^4\right] \pm O(\eta^3) \\ = 16\eta^2(4\sigma^2 + \mathbb{E}[(W_i \cdot \xi)^4]) \pm O(\eta^3). \end{aligned}$$

The only part which could significantly sway  $W_i$  is  $16\eta^2 \mathbb{E}[(W_i \cdot \xi)^4]$ , and indeed it does:

$$\begin{aligned} \mathbb{E}[(W_i \cdot \xi)^4] &= \sum_j W_{ij}^4 \mu_4 + 6 \sum_{j \neq j'} W_{ij}^2 W_{ij'}^2 \sigma^4 \\ &= \sum_j W_{ij}^4 (\mu_4 - 3\sigma^4) + 3 \left( \sigma^2 \sum_j W_{ij}^2 \right)^2 \\ &= 3\sigma^4 \left\|W_i\right\|_2^4 + \left\|W_i\right\|_4^4 (\mu_4 - 3\sigma^4). \end{aligned}$$

Eliminating the rotationally symmetric part, we obtain the implicit regularization-like term  $16\eta^2\sigma^4\|W_i\|_4^4\left(\frac{\mu_4}{\sigma^4}-3\right)$ , where  $\frac{\mu_4}{\sigma^4}-3$  is the excess kurtosis of the noise distribution  $\mathcal{D}$ . This means that when  $\mathcal{D}$  has negative excess kurtosis, this part of the loss will incentivize  $W_i$  to maximize its fourth norm  $\|W_i\|_4$ , which under the constraint that  $\|W_i\|_2 = 1$  means pushing towards sparsity: indeed,

- if  $W_{ij} = \pm\frac{1}{\sqrt{m}}$  for all  $j$  then  $\|W_i\|_4^4 = 1/m$ ,
- while if  $W_{ij} = \pm 1$  for some  $j$  and 0 elsewhere then  $\|W_i\|_4^4 = 1$ .

Thus, in summary we find that:

- Under our hypotheses, we easily obtain that the gradient on input  $e_i$  at the  $t^{\text{th}}$  step is  $\frac{\partial\mathcal{L}}{\partial W_i} = 2(W_i \cdot \xi)(2W_i + \xi)$  (details in ??), and therefore the update is given as  $W_i^{(t+1)} = W_i^{(t)} - 2\eta(W_i \cdot \xi)(2W_i + \xi)$ .
- Plugging this into the error  $W_i^{(t+1)} \cdot (W_i^{(t+1)} + \xi') - 1$  at the  $(t+1)^{\text{th}}$  step, we observe that the expected loss at the  $(t+1)^{\text{th}}$  is mostly made out of rotationally symmetric terms (which involve only constants and  $l_2$  norms  $\|W_i\|_2$ ) and lower-order terms, but there is one significant and interesting term which appears due to an interaction with the noise at either steps and takes the form  $16\eta^2\mathbb{E}[(W_i \cdot \xi)^4] = 3\sigma^4 16\eta^2\left(\|W_i\|_2^4 + \|W_i\|_4^4(\mu_4 - 3\sigma^4)\right)$ .